ACS APPLIED MATERIALS & INTERFACES

Research Article

www.acsami.org

Composition and Evolution of the Solid-Electrolyte Interphase in $Na_2Ti_3O_7$ Electrodes for Na-Ion Batteries: XPS and Auger Parameter Analysis

Miguel A. Muñoz-Márquez,*[,†] Maider Zarrabeitia,[†] Elizabeth Castillo-Martínez,[†] Aitor Eguía-Barrio,[‡] Teófilo Rojo,[†,‡] and Montse Casas-Cabanas[†]

[†]CIC Energigune, Parque Tecnológico de Álava, Albert Einstein 48, 01510 Miñano, Spain

[‡]Departamento de Química Inorgánica, Universidad del País Vasco UPV/EHU, 48080 Bilbao, Spain

Supporting Information

ABSTRACT: $Na_2Ti_3O_7$ is considered a promising negative electrode for Na-ion batteries; however, poor capacity retention has been reported and the stability of the solid-electrolyte interphase (SEI) could be one of the main actors of this underperformance. The composition and evolution of the SEI in $Na_2Ti_3O_7$ electrodes is hereby studied by means of X-ray photoelectron spectroscopy (XPS). To overcome typical XPS limitations in the photoelectron energy assignments, the analysis of the Auger parameter is here proposed for the first time in battery materials characterization. We have found that the electrode/electrolyte interface formed upon discharge, mostly composed by carbonates and semicarbonates (Na_2CO_3, $NaCO_3R$), fluorides (NaF), chlorides (NaCl) and poly(ethylene oxide)s, is unstable upon electrochemical cycling. Additionally, solid state nuclear magnetic resonance (NMR) studies prove the reaction of the polyvinylidene difluoride (PVdF) binder with sodium. The powerful approach used in this work, namely Auger parameter study, enables us to correctly determine the composition of the electrode surface layer without any interference from surface charging or absolute binding energy calibration effects. As a result, the suitability for Na-ion batteries of binders and electrolytes widely used for Li-ion batteries is questioned here.

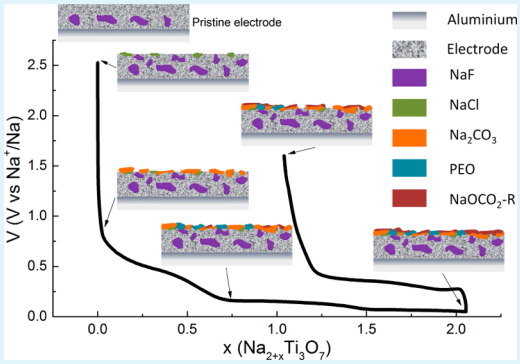

KEYWORDS: *XPS, Auger parameter, solid-electrolyte interphase, Na-ion battery, $Na_2Ti_3O_7$*

1. INTRODUCTION

Ever since the solid electrolyte interphase (SEI) model was described in 1979,[1] many investigations have been focused on the study of the morphology, composition, properties and electrochemical behavior of the SEI in Li-ion batteries.[2] An anode with an electrochemical potential (μ_A) above the electrolyte lowest unoccupied molecular orbital (LUMO) will reduce the electrolyte. Therefore, unless the μ_A is matched to the electrolyte LUMO, a stable passivating SEI layer is needed that prevents electron transfer and continuous electrolyte degradation, while it allows a fast ionic conductance from the anode to the electrolyte.[3] Typically, SEI formation leads to a reduction of the battery capacity affecting its lifetime; although, at the same time, its passivating properties are crucial for the electrode stability and, ultimately, for the correct battery operation.[4]

Na-ion batteries (NIB) are becoming more and more interesting due to their great potential for low cost stationary applications.[5,6] In fact, as reported in a very recent review,[7] several studies have been published regarding the composition of the SEI in NIB anodes such as hard-carbons,[8,9] Sn,[10] Cu_2Sb[11] and SnSb-porous carbon nanofiber electrodes.[12] In 2011, $Na_2Ti_3O_7$, was reported to reversibly react with Na ions at a very low voltage[13] and was followed by more studies on this[14,15] and other titanates.[16] However, despite the efforts on finding a good combination of electrolyte and binder for $Na_2Ti_3O_7$, electrode capacity fading is unavoidably obtained in all cases. The formation of a thin SEI in $Na_2Ti_3O_7$ was recently reported by a combined transmission electron microscopy (TEM) and Fourier transform infrared spectroscopy (FTIR) study.[17]

We report herein a thorough study on the composition and evolution of the SEI layer formed on $Na_2Ti_3O_7$ electrodes upon electrochemical cycling. X-ray photoelectron spectroscopy (XPS) measurements at different states of charge on electrodes never exposed to air have revealed the SEI composition as well as its instability upon cycling. Complementary solid state nuclear magnetic resonance (NMR) studies have proved the degradation of the PVdF binder.

Received: February 11, 2015
Accepted: March 26, 2015
Published: March 26, 2015

DOI: 10.1021/acsami.5b01375
ACS Appl. Mater. Interfaces 2015, 7, 7801−7808

2. EXPERIMENTAL SECTION

2.1. Electrode Preparation. The electroactive material, $Na_2Ti_3O_7$, was synthesized in-house via a ceramic route from precursors: anatase titanium oxide (99.9%, Alfa Aesar) and sodium carbonate monohydrate (>99.5%, Aldrich) as reported previously by Senguttuvan and co-workers.[13] Structural characterization of the sodium titanate was accomplished by means of X-ray diffraction (XRD) using a Bruker D8 diffractometer with a Cu Kα source. According to the XRD pattern shown in Figure S1 of the Supporting Information, the diffraction peaks of the synthesized material match very well with those of $Na_2Ti_3O_7$, space group $P2_1/m$. The phase purity is evidenced by the good fit and the refined cell parameters are in close agreement with those reported in the literature,[13] c.f. Table S1 of the Supporting Information. Electrodes were prepared by mixing the synthesized sodium titanate with carbon (C65) and polyvinylidene difluoride (PVdF, Solef 5130) in the weight ratio 88:10:2. Electrodes were coated on Al foil and dried at 80 °C in a vacuum oven for 24 h, pressed at 5 ton and vacuum-dried for 2 h at 80 °C.

2.2. Electrochemical Measurements. Swagelok cells were assembled in an Ar-filled glovebox using metallic sodium as negative and reference electrode and glass fiber disk separators. 1 M $NaClO_4$ (Fischer Scientific) in a mixture (1:1) of ethylene carbonate and propylene carbonate (EC, PC, Acros Organics) was used as the electrolyte, which is the most studied configuration.[13−15] Electrochemical tests of the assembled cells were performed at 25 °C using a VMP3 potentiostat (Bio-Logic SAS) at C/10 in the 0.05 to 1.6 V range. The charge/discharge profiles are shown in Figure 1a.

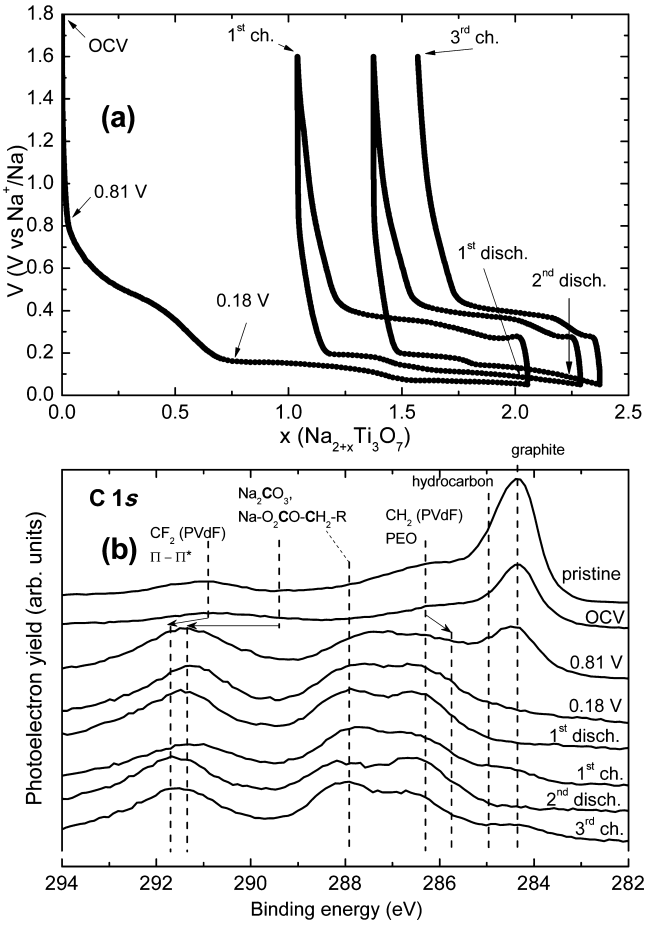

Figure 1. (a) Electrochemical potential profile of $Na_2Ti_3O_7$ electrodes during the first three cycles, points where XPS analysis is performed are pointed with arrows. (b) C 1s XPS core level spectra for electrodes before cycling and at points of the charge/discharge curve indicated in panel a.

2.3. X-ray Photoelectron Spectroscopy (XPS). Electrode surface was investigated at different charge states using a Phoibos 150 XPS spectrometer and a nonmonochromatic Mg Kα source ($h\nu$ = 1253.6 eV). Electrodes were inserted into the XPS vacuum chamber using an Ar-filled transfer system. Cycled electrodes were rinsed with PC prior to XPS experiments. High resolution scans were acquired at 100 W, 20 eV pass energy and 0.1 eV energy step. Depth profiling was done using a focused ion gun for 1 keV Ar^+ with a sputtering rate of 0.2 Å/s, which was determined from measurements in a Ta_2O_5 standard calibrated with laser profilometry and corrected by the relative sputtering cross section of our particular compound. X-ray beam and ion beam power and energy were tested in reference samples to minimize the sample damage. For the five samples where the graphitic carbon peak is visible, calibration of the binding energy scale was set using the reference at 284.4 eV, for the other three samples, the same shift measured for the previous five was used; it is well-known that in Li-ion batteries this would not be possible because the Li ions insert into the graphite structure to form Li_xC_6 that results in a lower binding energy of the C−C bond; however, as reported up to date, Na ions do not insert into graphite and they do so into hard-carbon only.[8,18] Therefore, selecting the graphite peak as the reference for the binding energy reference is the best option.

However, due to differential surface charging effects, the aforementioned calibration procedure is not sufficient for a full determination of the surface layer composition. As it will be discussed later, the evaluation of the Auger parameter will provide crucial information on this regard, for this, the Na $KL_{23}L_{23}$ peaks were also measured and along with the photoelectron Na 1s peak were fitted using the CasaXPS software. Voigt functions (70% Gaussian and 30% Lorentzian) were used in the fits to determine the peak positions, the fitting parameters were obtained using a Levenberg−Marquardt optimization algorithm starting from different initial guess parameters that always led to the same result.

2.3. Solid State Nuclear Magnetic Resonance (NMR). Solid state NMR experiments were performed to check the binder degradation; electrodes were scratched out of the aluminum current collector and the powders of the soaked and discharged electrodes were fitted into the rotors inside an Ar-filled glovebox. ^{19}F solid state NMR data were collected on a Bruker 500 MHz spectrometer, at an operating frequency of 470 MHz, with a 1.3 mm probe. Rotors were spun at a magic-angle-spinning (MAS) rate of 50 kHz. A rotor synchronized Hahn echo (90°-τ-180°-τ-acq.) sequence was used with a 90° pulse of 3.6 μs and a delay of 40 s. Spectra are referenced to secondary LiF (−201 ppm).[19] Approximately 100 000 scans were collected per ^{19}F solid-state NMR spectrum.

3. RESULTS AND DISCUSSION

The SEI formation and evolution was followed by XPS from the Cl 2p, C 1s, O 1s, F 1s, Na 1s photoelectron peaks and Na $KL_{23}L_{23}$ Auger peaks. Among these, the most important photoemission line was the C 1s peak (Figure 1b) recorded at different voltage values during discharge/charge, as shown in the profiles of Figure 1a. The assignments of the C 1s components have been done on the basis of previous XPS studies of carbon-based materials.[20] Because there are different possibilities for C−O bonds on the surface of graphitic materials, the peak energies will be assigned following the trends reported by Xie and Sherwood.[21] However, absolute binding energies for cycled electrodes are slightly different to the ones reported in the literature for reference materials, the reason being the nonuniform charging effects of nonconducting microdomains of salt residuals and reduction products on the surface. XPS data of reference compounds such as PVdF, C65 carbon, $NaClO_4$ and Na_2CO_3, along with their internal energy shifts, were collected to corroborate the peak assignment. Finally, the majority of peaks could be assigned from relative peak positions obtained from binding energy differences[22] and

DOI: 10.1021/acsami.5b01375
ACS Appl. Mater. Interfaces 2015, 7, 7801−7808

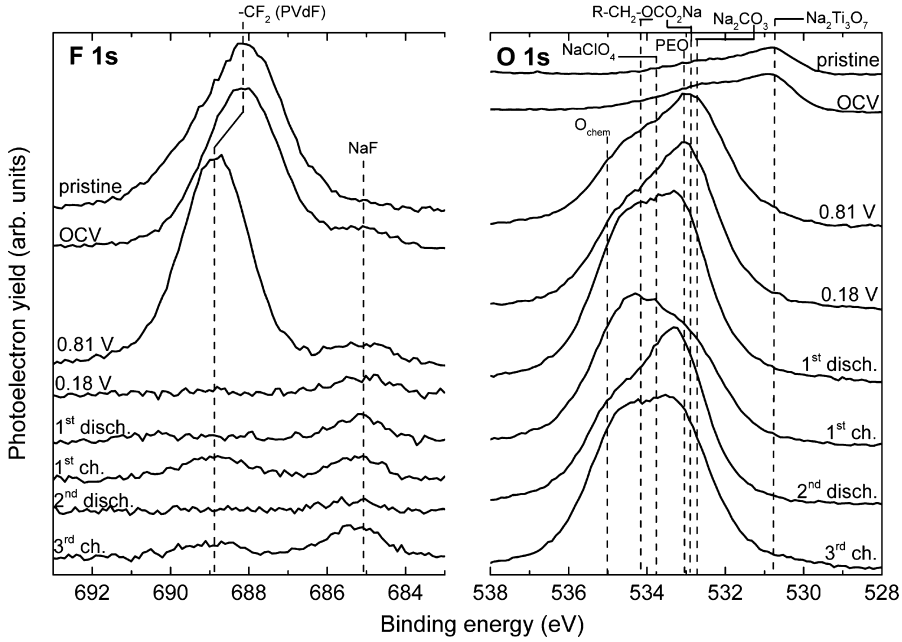

Figure 2. XPS F 1s and O 1s spectra are shown for pristine electrodes and at different charge states.

after calculation of the corresponding Auger parameter[23] which, involving measurements of both Auger and photoelectron line energies, provides abundant chemical state information without the necessity or concern for charge correction and work function measurements. In Table S2 of the Supporting Information, experimental data of photoemission lines and Auger parameters from reference samples measured in our XPS are available.

One of the key features in the C 1s photoelectron spectra of the pristine and OCV electrodes is the component at 284.4 eV assigned to graphitic-like compounds with a marked asymmetry toward high binding energies due to the presence of C−C and C−H bonds from hydrocarbon contamination and from the excitation of electron−hole pairs,[24] the asymmetry in the latter case will depend on the density of states at the Fermi level and it could mask the real contribution from hydrocarbon contamination, which most probably is overestimated. In the 290.5−290.8 eV range, contributions from organic carbonate contamination and a shake-up feature corresponding to a Π−Π* transition from graphitic-like compounds will appear.[25] The graphitic-like component in the XPS spectra of the pristine and OCV electrodes mainly corresponds to the conductive additive. The presence of polyvinylidene difluoride (PVdF, $-(CF_2-CH_2)_n-$) in the pristine and OCV samples is revealed by two equal peaks, one at 286.4 eV from the $-CH_2$ and another one at 290.9 eV from the fluorinated carbon, overlapped with the Π−Π* transition.[26] As the sodiation process evolves, the graphitic-like signal decreases. Indeed, the peak at 284.4 eV progressively disappears upon discharge between 0.6 and 0.2 V until its complete extinction at 0.18 V, showing the formation of a SEI layer that completely covers the electrode surface. Based on the empirical relationship between the escape length of a photoelectron and its kinetic energy, these results are consistent with a minimum SEI layer thickness of 5 nm for photoelectrons with a kinetic energy around 1000 eV.[27,28] Upon charge, a small shoulder appears at 284.4 eV from the underlying graphitic carbon indicating a thinning or cracking of the SEI layer. After a second discharge, the shoulder disappears as the SEI layer regenerates fully covering the electrode surface again. This process of SEI formation upon discharge and partial dissolution upon charge is repeated along several cycles, shortly after, the capacity fade is too large and the cell stops working (not shown).

As the graphitic-like component disappears during discharge, other components become more prominent: carbon atoms surrounded by one oxygen atom such as sodium alkoxides (NaOR) and poly(ethylene oxide) $(-CH_2-CH_2-O-)_n$ oligomers (PEO) at 286.1−286.5 eV;[12,22] and carbons in a three-oxygen environment like sodium alkyl carbonates ($NaCO_3R$, R = different long-chain alkyl groups)[29] and sodium carbonate (Na_2CO_3) with contributions at 291−291.5 eV[22] instead of 289.4 eV[11] due to differential charging effects. The presence of $NaCO_3R$ involves an additional feature at 287.5−288 eV originated by the first carbon atom in the alkane chain.[12,22] Finally, concerning the evolution of the C 1s PVdF components during cycling, it has been previously reported[30] that sodium atoms can chemically interact with PVdF strongly influencing the fluorine electronic structure, but perturbing the carbon backbone only slightly by additionally splitting the $-CF_2$ and $-CH_2$ components, as indicated in Figure 1b.

The study of the XPS F 1s and O 1s peaks allow us a better understanding of the surface layer composition (Figure 2). In the F 1s photoelectron line, a faint peak corresponding to NaF (685 eV) appears as soon as the electrode and electrolyte are assembled. Typically, this is a consequence of a dehydrofluorination reaction in the PVdF binder that results in NaF formation, as it has been previously reported for Li-ion batteries.[31] To fully confirm the NaF formation, we performed ^{19}F solid state NMR experiments on several electrodes, as shown in Figure 3; in panels b, c and d of this figure, the formation of NaF (−221 ppm)[19] is revealed even in the pristine electrode (Figure 3b), indicating that sodium fluoride is initially formed in the bulk region during electrode preparation because no traces are detected in the surface by XPS. After comparing the relative peak intensities within the same NMR spectra, taking the PVdF intensity as a reference, we can conclude that

DOI: 10.1021/acsami.5b01375
ACS Appl. Mater. Interfaces 2015, 7, 7801−7808

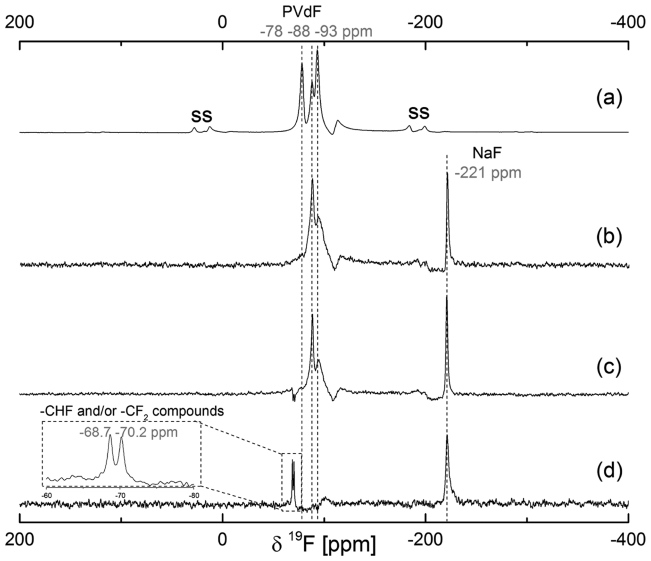

Figure 3. ^{19}F MAS NMR spectra of (a) PVdF reference sample, (b) pristine $Na_2Ti_3O_7$ electrode, (c) electrode at OCV and (d) electrode discharged down to 0.05 V vs Na^+/Na. The inset in panel d shows details of the evolution of the PVdF signal into CHF- and CF_2-based compounds. Spinning side bands of the most intense isotropic signals are labeled as "ss".

the intensity of the NaF peak increases upon discharge. Going back to the XPS results, the main peak in the F 1s spectrum corresponds to $-CF_2$ groups from PVdF (688.15 eV) in the pristine and OCV electrodes.[26] However, as observed in the C 1s spectrum, the $-CF_2$ component in the F 1s spectrum evolves toward higher binding energies upon discharge as a result of surface charging and final state effects, such as screening induced by Na doping that involves changes in the intensity and core level binding energy shift.[30] The evolution of the PVdF was further confirmed by our NMR experiments of the discharged electrode compared to a PVdF reference sample (Figure 3a,d). The disappearance of the NMR signals at −78, −88 and −93 ppm, typical from PVdF,[32] and the appearance of a very narrow doublet at −68 and −70 ppm in the NMR spectrum of the discharged electrode indicates the presence of residual −CHF and/or $-CF_2$ bonding resulting from the degradation of PVdF. This lack of stability toward sodium doping could be one of the factors affecting the larger capacity fade of PVdF-based titanate electrodes when compared with other binders such as sodium alginate[17] which are still affected by capacity fading. In the F 1s XPS spectrum (Figure 2), the $-CF_2$ component of the PVdF disappears after the SEI formation at 0.18 V and partially reappears after every charge step. Although this cyclic behavior is only clear after the first discharge for NaF and considering that signal-to-noise ratio for the fluorine spectrum is rather poor, the global trend of the F 1s spectrum would agree with a partial dissolution of the SEI layer.

As it can be seen in the right panel of Figure 2, the O 1s spectrum from the pristine and OCV electrodes has a dominating component at ∼531 eV that corresponds to $Na_2Ti_3O_7$; this main component is extended toward higher binding energies (531−531.5 eV) due to the presence of hydroxides. The secondary peak at 532−533 eV can be attributed to some residual amount of carbonates, moisture and, for the OCV sample, also some $NaClO_4$ residuals. As the electrode starts its discharge, a thick layer covering the electrode surface is quickly formed that is composed of sodium carbonate (∼532.8 eV) and alkylcarbonate (∼534 eV and ∼532.9 eV), along with PEO (∼533 eV), which consolidates upon discharge.[22] The PEO results from direct polymerization of EC where alkylcarbonates could act as catalysts.[33,34] In the 531.5−532.5 eV range, the sodium alkoxide should also appear, but given the overlapping with other components, it is very difficult to determine its existence.[35] Taking into account the measured shift between the O 1s and Cl 2p peaks in a $NaClO_4$ reference sample, the contribution from traces of $NaClO_4$ would appear at 533.8 eV in this case. At ∼535 eV, there is a component that corresponds to an overlayer of chemisorbed oxygen[21] as a result of the perchlorate anion dissociation.[36] The PEO contribution in the O 1s spectrum is attenuated upon charge, in agreement with the observed behavior of the PEO component at 286.5 eV in the C 1s peak, indicating a partial dissolution of this species. However, carbonate, alkoxide, alkylcarbonate and PEO signals are very close to each other and it is very difficult to establish that only PEO is dissolved upon charge. Conventional XPS analysis is not sufficient to obtain a complete picture of the SEI evolution; therefore, the study of the Auger parameter will be crucial to go one step further, enabling us to identify components of the SEI and their stability during electrochemical cycling.

XPS measurements of the Cl 2p level (Figure 4, bottom panel) show traces of $NaClO_4$ in the electrode surface; however, as it will be discussed later, one of the most striking features is the NaCl formed spontaneously at OCV. The photoinduced decomposition of sodium perchlorate and sodium chlorate has been previously studied[36] and, indeed, part of the NaCl observed could be a result of a decomposition

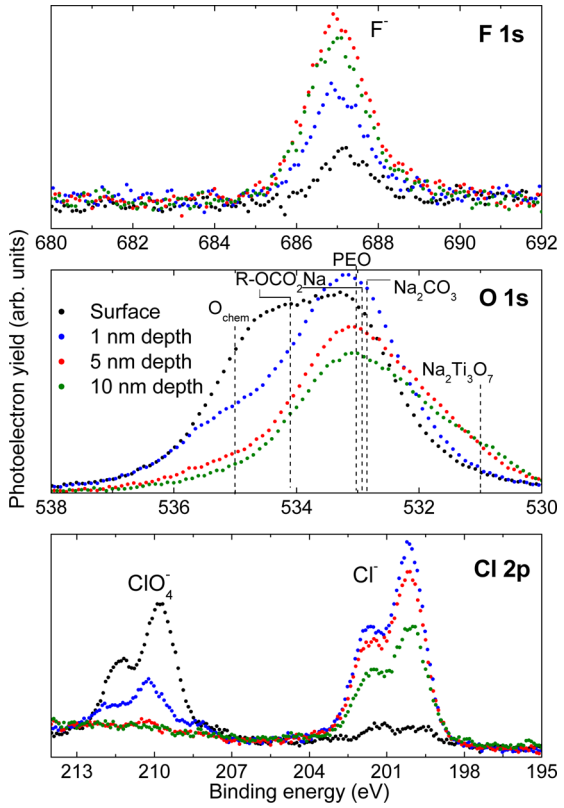

Figure 4. XPS spectra (F 1s, O 1s and Cl 2p) at different depths of a discharged electrode: outermost surface (black) and after removing 1 nm (blue), 5 nm (red) and 10 nm (green) with Ar^+ bombardment.

DOI: 10.1021/acsami.5b01375
ACS Appl. Mater. Interfaces 2015, 7, 7801−7808

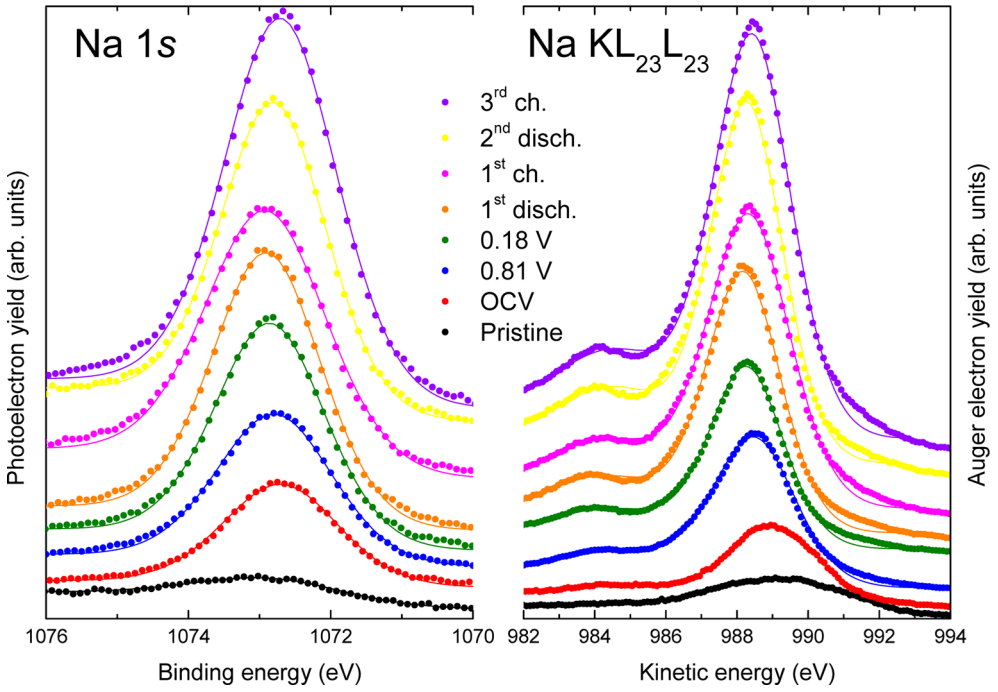

Figure 5. XPS data from Na in $Na_2Ti_3O_7$ electrodes at different charge states. On the left panel is the 1s photoemission line and on the right panel the Auger $KL_{23}L_{23}$ transition. The circles correspond to the experimental data and the solid lines are the fits; all curves are color coded according to their charge state.

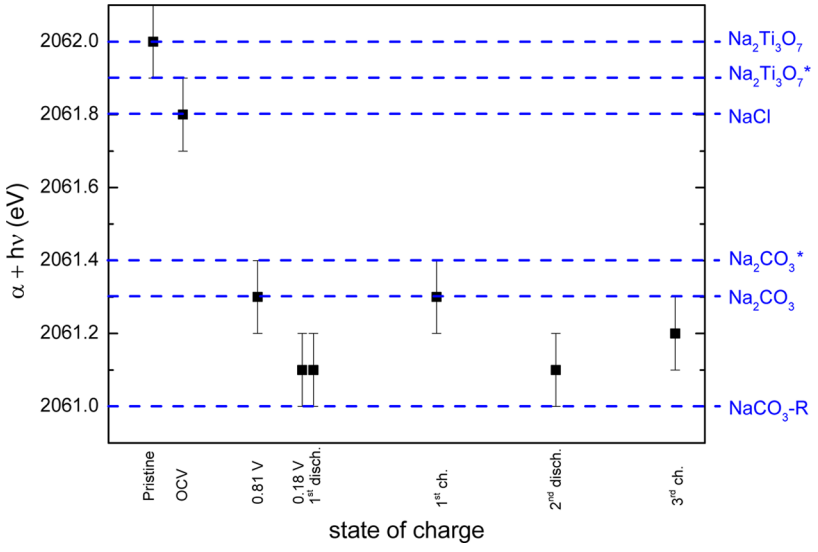

Figure 6. Modified Auger parameter ($\alpha + h\nu = E_K(KL_{23}L_{23}) + E_B(1s)$) for sodium at different states of charge of the electrode. Reference values obtained directly from measuring a reference sample (*) or from ref 37.

of the perchlorate induced by the Mg Kα radiation from the XPS source. However, in our study, we carefully screened different low power X-ray beam conditions to partially avoid this problem. As a result, the Cl 2p level measured at different charge states reveals the presence of NaCl at OCV, whereas the dominant component in the electrochemically cycled samples corresponds to $NaClO_4$ traces not removed during the electrode washing (Figure S2 of the Supporting Information). This points out the spontaneous formation of NaCl at the very beginning of electrode preparation prior to any cycling, which will then be buried by the other SEI components such as carbonates and alkylcarbonates.

As previously mentioned, the full identification of the SEI composition is rather complicated, the main reasons being the overlapping of several components in the photoelectron peaks along with partial surface charging and the difficulties to establish an absolute binding energy calibration. To overcome these limitations, an approach never used before for the characterization of the SEI layer is herein proposed. This consists in the analysis of the Auger parameter (α) for Na, which results from determining the energy shift between the Na 1s photoelectron line and the Na $KL_{23}L_{23}$ Auger line, which is a doubly ionized final state more sensitive to chemical shifts. Indeed, the analysis of the Auger parameter is hampered in Li-based compounds because the Auger lines are not easily

DOI: 10.1021/acsami.5b01375
ACS Appl. Mater. Interfaces 2015, 7, 7801−7808

reachable by XPS. However, for Na-based compounds, it turns out to be a very powerful tool. In Figure 5, the fits used to determine the positions of the Na 1s and Na $KL_{23}L_{23}$ peaks are shown. Once the peak positions are known from the fits, the Auger parameter is calculated; all these results are included in Table S3 of the Supporting Information. The outcome of this analysis is shown in Figure 6, and the measured values with the corresponding compound assignation can be found in Table 1.

Table 1. Experimental Auger Parameters of the Na-based Compounds of the SEI Layer at Different Charge States along with Their Assignation

charge state	modified Auger parameter (eV)[a]	compound
pristine	2062.0	$Na_2Ti_3O_7$[b]
OCV	2061.8	NaCl
0.81 V	2061.3	Na_2CO_3
0.18 V	2061.1	Na_2CO_3 + $NaCO_3$-R[b]
1st discharge	2061.1	Na_2CO_3 + $NaCO_3$-R
1st charge	2061.3	Na_2CO_3
2nd discharge	2061.1	Na_2CO_3 + $NaCO_3$-R
3rd charge	2061.2	Na_2CO_3 + $NaCO_3$-R

[a] $\alpha + h\nu = E_K(KL_{23}L_{23}) + E_B(1s)$. [b] Approximate values extrapolated from ref 37.

Because we are dealing with a high binding energy photoelectron line, namely Na 1s, the detected photoelectrons will have a very low kinetic energy and a very short inelastic mean free path; therefore, the resulting peak will be integrated over the outermost surface region. This means that surface sensitivity will be enhanced if compared with other elements such as Cl, C, O and F. This anticipates the fact that with the Auger parameter the presence of subsurface NaF cannot be detected, although its presence was previously confirmed by F 1s XPS and ^{19}F NMR measurements. In Figure 6, the Auger parameter is plotted for different states of charge of the electrode. The Auger parameter for the pristine and OCV electrodes nicely fits with the presence of $Na_2Ti_3O_7$ and NaCl, respectively.[37] The NaCl formation is thus further confirmed by the analysis of the determined Auger parameter on the OCV sample. Upon discharge, the formation of Na_2CO_3 is quickly evidenced covering any trace of NaCl. Later, at voltages below 0.2 V, the carbonate itself is partially covered by an alkylcarbonate layer that is partially dissolved upon charge as corroborated by Auger parameters that show again the presence of sodium carbonate. This is a cyclic behavior that agrees with the evolution of the O 1s photoelectron peak.

Once the composition of the surface layer was known, we sought for a better understanding of its structure by performing an XPS depth profiling using a 1 keV Ar ion beam (Figure 4). After the F 1s, O 1s and Cl 2p signals were observed at different depths in a discharged electrode, it was observed that, as expected, the NaF peak intensity increases in the subsurface region, the chemisorbed oxygen and alkylcarbonate overlayer disappears after a few seconds of ion bombardment and, finally, the NaCl concentration increases in the subsurface region while residual $NaClO_4$ is removed from the surface. From the depth profiling results shown in Figure 4 and the Auger parameter analysis from Figures 5 and 6, it can be clearly determined that chemisorbed oxygen and alkylcarbonate are in the outermost surface region coexisting with PEO partially buried. This overlayer is covering a rough layer of carbonates that has grown on top of the spontaneously formed NaCl and NaF. At the same time, it could be initially concluded that the observed signal increase for NaF could also be due to the removal of the residual $NaClO_4$ overlayer. However, the NMR experiment indicates that a significant concentration of NaF is present, although it cannot be fully detected by XPS due to its location in a buried region of the electrode. Subsequent ion bombardment in the discharged electrode shows that the SEI layer thickness is around 5−10 nm, as initially estimated from the photoelectron escape length. After 5 nm of the surface is removed, the signals of the NaF and NaCl significantly decrease while the component corresponding to the $Na_2Ti_3O_7$ appears at 531 eV in the O 1s spectrum: a clear sign of SEI removal. At this point, if we keep etching the surface beyond 10 nm, other compounds not detected at the initial stages of discharge could be induced by the ion, so we cannot fully conclude anything about the SEI composition beyond this point. Certainly, ion beam induced surface damage is something that has to be considered for long sputtering processes, i.e., more than 1 nm.

4. CONCLUSIONS

The instability upon charge of the SEI formed in $Na_2Ti_3O_7$ electrodes has been observed for the first time. Despite the galvanostatic curves only show a feature of SEI formation at the first discharge (Figure 1a), the SEI is partially dissolved upon every charge. This surface layer is composed of a thin overlayer of chemisorbed oxygen, alkylcarbonates and PEO that covers the solid layer of sodium carbonates, NaF and NaCl (∼5 nm), being the NaCl formed spontaneously at the beginning (OCV) by decomposition of the electrolyte salt. The NaF is formed during electrode preparation having its origin in the PVdF dehydrofluorination reactions. In contrast to the SEI in Li-ion batteries, the SEI formed in $Na_2Ti_3O_7$ electrodes is thinner and has more inorganic components than organic ones, with PEO and alkylcarbonates being partially soluble and originating a continuous SEI reformation. The predominance of inorganic compounds in the SEI agrees with the SEI composition in hard-carbon anodes; meanwhile, the thinning or cracking of the SEI has been reported for Sn- and Sb-based anodes. In our case, reactions of the PVdF binder have also been spotted as demonstrated by NMR and XPS experiments, indirectly through formation of NaF as a result of the HF formation by dehydrofluorination of the PVdF and directly through the evolution of the $-CF_2$ groups. The observed SEI instability involves a continuous electrolyte degradation which along with the binder degradation will certainly contribute to the observed capacity fade and reduced cycle life. Identification of compounds and their evolution has been possible thanks to the analysis of the Auger parameter, applied for the first time to the SEI study, which has provided clear information where conventional XPS analysis was not sufficient for a correct binding energy assignment.

The current electrode formulation in terms of binder and electrolyte is far from ideal, although the Li counterparts have been proven to work with Li-ion batteries. Several alternatives have been proposed in the literature for this and other electrode materials, namely binders such as sodium alginate-(NaAlg) or sodium carboxymethylcellulose (Na-CMC) and electrolytes such as $NaBF_4$, $NaPF_6$ and NaTFSI; still, their performance is not comparable to their Li counterparts. For sodium titanate electrodes, all the efforts have been focused on the use of NaAlg and PVdF along with $NaClO_4$ or NaFSI,[17] the obtained performance results are pretty similar in all cases and capacity fades dramatically before 20 cycles. We consider that

DOI: 10.1021/acsami.5b01375
ACS Appl. Mater. Interfaces 2015, 7, 7801−7808

the higher reactivity of Na compared with Li and the catalytic activity of titanate materials might be among the factors influencing the underperformance of binders and electrolytes. To improve the $Na_2Ti_3O_7$ performance, the exploration of protective coatings for the electrode active material might result in a decrease of the catalytic activity of the titanate rendering the system more stable.

■ ASSOCIATED CONTENT

Supporting Information

(Figure S1) XRD data, (Figure S2) XPS data of the Cl 2p photoelectron peak, (Table S1) Rietveld refinement results, (Table S2) XPS results from reference samples, (Table S3) experimental Auger parameters. This material is available free of charge via the Internet at http://pubs.acs.org.

■ AUTHOR INFORMATION

Corresponding Author

*M. A. Muñoz-Márquez. E-mail: mamunoz@cicenergigune.com.

Notes

The authors declare no competing financial interest.

■ ACKNOWLEDGMENTS

The authors thank M. R. Palacín and M. Armand for fruitful discussions. This work was funded by the Basque Government through Etortek CICenergiGUNE 10 and by the Ministerio de Economía y Competitividad of the Spanish Government (Project ENE2013-44330-R). M. Zarrabeitia and A. Eguía-Barrio thank the Basque Government and the UPV/EHU respectively for their Ph.D. fellowships.

■ REFERENCES

(1) Peled, E. The Electrochemical-Behavior of Alkali and Alkaline-Earth Metals in Non-aqueous Battery Systems - The Solid Electrolyte Interphase Model. *J. Electrochem. Soc.* **1979**, *126*, 2047−2051.

(2) *Lithium-Ion Batteries Solid-Electrolyte Interphase*; Balbuena, P., Wang, Y., Eds.; Imperial College Press: London, 2004.

(3) Goodenough, J.; Kim, Y. Challenges for Rechargeable Li-Ion Batteries. *Chem. Mater.* **2010**, *22*, 587−603.

(4) Vetter, J.; Novák, P.; Wagner, M.; Veit, C.; Moller, K.; Besenhard, J.; Winter, M.; Wohlfahrt-Mehrens, M.; Vogler, C.; Hammouche, A. Ageing Mechanisms in Lithium-Ion Batteries. *J. Power Sources* **2005**, *147*, 269−281.

(5) Zhou, H. New Energy Storage Devices for Post Lithium-Ion Batteries. *Energy Environ. Sci.* **2013**, *6*, 2256.

(6) Palomares, V.; Casas-Cabanas, M.; Castillo-Martínez, E.; Han, M. H.; Rojo, T. Update on Na-based Battery Materials. A Growing Research Path. *Energy Environ. Sci.* **2013**, *6*, 2312−2337.

(7) Ponrouch, A.; Monti, D.; Boschin, A.; Steen, B.; Johansson, P.; Palacín, M. R. Non-aqueous Electrolytes for Sodium-Ion Batteries. *J. Mater. Chem. A* **2015**, *3*, 22−42.

(8) Komaba, S.; Murata, W.; Ishikawa, T.; Yabuuchi, N.; Ozeki, T.; Nakayama, T.; Ogata, A.; Gotoh, K.; Fujiwara, K. Electrochemical Na Insertion and Solid Electrolyte Interphase for Hard-Carbon Electrodes and Application to Na-Ion Batteries. *Adv. Funct. Mater.* **2011**, *21*, 3859−3867.

(9) Ponrouch, A.; Dedryvere, R.; Monti, D.; Demet, A. E.; Mba, J. M. A.; Croguennec, L.; Masquelier, C.; Johansson, P.; Palacín, M. R. Towards High Energy Density Sodium Ion Batteries through Electrolyte Optimization. *Energy Environ. Sci.* **2013**, *6*, 2361−2369.

(10) Baggetto, L.; Ganesh, P.; Meisner, R. P.; Uncoic, R. R.; Jumas, J.-C.; Bridges, C. A.; Veith, G. M. Characterization of Sodium Ion Electrochemical Reaction with Tin Anodes: Experiment and Theory. *J. Power Sources* **2013**, *234*, 48−59.

(11) Baggetto, L.; Allcorn, E.; Manthiram, A.; Veith, G. M. Cu_2Sb Thin films as Anode for Na-Ion Batteries. *Electrochem. Commun.* **2013**, *27*, 168−171.

(12) Ji, L.; Gu, M.; Shao, Y.; Li, X.; Engelhard, M. H.; Arey, B. W.; Wang, W.; Nie, Z.; Xiao, J.; Wang, C.; Zhang, J.-G.; Liu, J. Controlling SEI Formation on SnSb-Porous Carbon Nanofibers for Improved Na Ion Storage. *Adv. Mater.* **2014**, *26*, 2901−2908.

(13) Senguttuvan, P.; Rousse, G.; Seznec, V.; Tarascon, J.-M.; Palacín, M. R. $Na_2Ti_3O_7$: Lowest Voltage Ever Reported Oxide Insertion Electrode for Sodium Ion Batteries. *Chem. Mater.* **2011**, *23*, 4109−4111.

(14) Wang, W.; Yu, C.; Lin, Z.; Hou, J.; Zhu, H.; Jiao, S. Microspheric $Na_2Ti_3O_7$ Consisting of Tiny Nanotubes: An Anode Material for Sodium-Ion Batteries with Ultrafast Charge-Discharge Rates. *Nanoscale* **2013**, *5*, 594−599.

(15) Rudola, A.; Saravanan, K.; Mason, C.; Balaya, P. $Na_2Ti_3O_7$: An Intercalation based Anode for Sodium-Ion Battery Applications. *J. Mater. Chem. A* **2013**, *1*, 2653−2662.

(16) Doeff, M. M.; Cabana, J.; Shirpour, M. Titanate Anodes for Sodium Ion Batteries. *J. Inorg. Organomet. Polym.* **2014**, *24*, 5−14.

(17) Pan, H.; Lu, X.; Yu, X.; Hu, Y.-S.; Li, H.; Yang, X.-Q.; Chen, L. Sodium Storage and Transport Properties in Layered $Na_2Ti_3O_7$ for Room-Temperature Sodium-Ion Batteries. *Adv. Energy Mater.* **2013**, *3*, 1186−1194.

(18) Xia, X.; Obrovac, M. N.; Dahn, J. R. Comparison of the Reactivity of Na_xC_6 and Li_xC_6 with Non-aqueous Solvents and Electrolytes. *Electrochem. Solid-State Lett.* **2011**, *14*, A130−A133.

(19) Groß, U.; Rüdiger, S.; Grimmer, A.-R.; Kemnitz, E. ^{19}F-NMR Solid State Investigations of Monovalent Alkali Metal Fluorides and Tetra-Alkylammonium Fluorides. *J. Fluorine Chem.* **2002**, *115*, 193−199.

(20) Sherwood, P. M. A. Surface Analysis of Carbon and Carbon Fibers for Composites. *J. Electron Spectrosc. Relat. Phenom.* **1996**, *81*, 319−342.

(21) Xie, Y. M.; Sherwood, P. M. A. X-ray Photoelectron-Spectroscopic Studies of Carbon-Fiber Surfaces. 12. The Effect of Microwave Plasma Treatment on Pitch-based Carbon-Fiber Surfaces. *Appl. Spectrosc.* **1990**, *44*, 797−803.

(22) Andersson, A. M.; Henningson, A.; Siegbahn, H.; Jansson, U.; Edström, K. Electrochemically Lithiated Graphite Characterised by Photoelectron Spectroscopy. *J. Power Sources* **2003**, *119*−*121*, 522−527.

(23) Wagner, C. D.; Joshi, A. The Auger Parameter, Its Utility and Advantages: A Review. *J. Electron Spectrosc. Relat. Phenom.* **1988**, *47*, 283−313.

(24) Blyth, R. I. R.; Buqa, H.; Netzer, F. P.; Ramsey, M. G.; Besenhard, J. O.; Golob, P.; Winter, M. XPS Studies of Graphite Electrode Materials for Lithium Ion Batteries. *Appl. Surf. Sci.* **2000**, *167*, 99−106.

(25) Bradshaw, A. M.; Cederbaum, S. L.; Domcke, W.; Krause, U. Plasmon Coupling to Core Hole Excitations in Carbon. *J. Phys. C: Solid State Phys.* **1974**, *7*, 4503−4512.

(26) Beamson, G.; Briggs, D. *High Resolution XPS of Organic Polymers: The Scienta ESCA300 Database*; John Wiley & Sons, Ltd: Chichester, U. K., 1992.

(27) Powell, C. Attenuation Lengths of Low-Energy Electrons in Solids. *Surf. Sci.* **1974**, *44*, 29−46.

(28) Woodruff, D. P.; Delchar, T. A. *Modern Techniques of Surface Science*, 2nd ed; Cambridge University Press: Cambridge, U. K., 1994.

(29) Aurbach, D.; Daroux, M. L.; Faugy, P. W.; Yeager, E. Identification of Surface-Films Formed on Lithium in Propylene Carbonate Solutions. *J. Electrochem. Soc.* **1987**, *134*, 1611−1620.

(30) Xu, B.; Choi, J.; Borca, C. N.; Dowben, P. A.; Sorokin, A. V.; Palto, S. P.; Petukhova, N. N.; Yudin, S. G. Comparison of Aluminium and Sodium Doped Poly(vinylidene fluoride-trifluoroethylene) Co-polymers by X-ray Photoemission Spectroscopy. *Appl. Phys. Lett.* **2001**, *78*, 448−450.

DOI: 10.1021/acsami.5b01375
ACS Appl. Mater. Interfaces 2015, 7, 7801−7808

(31) Crowe, R.; Badyal, J. P. S. Surface Modification of Poly-(vinylidene difluoride) (PVDF) by LiOH. *J. Chem. Soc., Chem. Commun.* **1991**, 958−959.
(32) Ando, S.; Harris, R. K.; Scheler, U. In *Encyclopedia of Nuclear Magnetic Resonance. Vol 9: Advances in NMR*; Grant, D. M., Harris, R. K., Eds.; John Wiley & Sons, Ltd: Chichester, U. K., 2002; pp 531−550.
(33) Genies, S.; Yazami, R.; Garden, J.; Frison, J. C. SEM and FT-IR Characterization of the Passivation Film on Lithiated Mesocarbon Fibers. *Synth. Met.* **1998**, *93*, 77−82.
(34) Vogdanis, L.; Heitz, W. Carbon-Dioxide as a Monomer 0.3. The Polymerization of Ethylene Carbonate. *Makromol. Chem., Rapid Commun.* **1986**, *7*, 543−547.
(35) Rendek, L. J.; Chottiner, G. S.; Scherson, D. The Reactivity of Linear Alkyl Carbonates Toward Metallic Lithium: X-ray Photoelectron Spectroscopy Studies in Ultrahigh Vacuum. *J. Electrochem. Soc.* **2002**, *149*, E408−E412.
(36) Copperthwaite, R.; Lloyd, J. Photoinduced Decomposition of Sodium Perchlorate and Sodium Chlorate when Studied by X-ray Photoelectron Spectroscopy. *J. Chem. Soc., Dalton Trans.* **1977**, 1117−1121.
(37) Wagner, C. D.; Riggs, W. M.; Davis, L. E.; Moulder, J. F. *Handbook of X-ray Photoelectron Spectroscopy*; Perkin-Elmer Corp., Physical Electronics Division: Eden Praire, MN, 1979.

DOI: 10.1021/acsami.5b01375
ACS Appl. Mater. Interfaces 2015, 7, 7801−7808